Effect of thermal treatment on Zn nanodisks

Pedro E. Acuña-Avila, Roberto López, Enrique Vigueras-Santiago, Susana Hernández-López, Marco Camacho-López, Carlos Ornelas-Gutierrez, and Wilber Antunez

Citation: AIP Advances **5**, 067109 (2015); doi: 10.1063/1.4922214

View online: https://doi.org/10.1063/1.4922214

View Table of Contents: http://aip.scitation.org/toc/adv/5/6

Published by the American Institute of Physics

Effect of thermal treatment on Zn nanodisks

Pedro E. Acuña-Avila,[1,a] Roberto López,[1] Enrique Vigueras-Santiago,[1]
Susana Hernández-López,[1] Marco Camacho-López,[1]
Carlos Ornelas-Gutierrez,[2] and Wilber Antunez[2]
[1]*Laboratorio de Investigación y Desarrollo de Materiales Avanzados (LIDMA). Facultad de Química de la Universidad Autónoma del Estado de México. Paseo Colón esquina Paseo Tollocan C.P. 50120, Toluca, Estado de México, México*
[2]*Centro de investigación en Materiales Avanzados S. C. (CIMAV). Miguel de Cervantes N° 120. C.P. 31109. Chihuahua, Chihuahua, México*

(Received 13 April 2015; accepted 24 May 2015; published online 2 June 2015)

Metallic Zn nanodisks with hexagonal morphology were obtained onto glass substrate under vacuum thermal evaporation. A thermal characterization of Zn nanodiks showed a lower oxidation temperature than source powder Zn. Different thermal treatment on Zn nanodisks played an important role on the morphology, crystal size and surface vibrational modes of ZnO. The growth of ZnO nanoneedles started at the edge of metallic zinc hexagonal structures according with SEM images, the higher temperature the longer needles were grown. XRD diffractogram confirmed the wurtzite structure of ZnO with metallic nuclei. A wide band between 530 and 580 cm^{-1} of Raman scattering corresponded at surface vibrational modes not observed at higher temperature. [http://dx.doi.org/10.1063/1.4922214]

I. INTRODUCTION

It is well known that a lot of oxide metallic semiconductors like SnO_2, TiO_2 and ZnO can be useful in electronic devices as gas sensors[1–3] due to changes on electrical conductivity when they are exposed to reducing or oxidizing gases. ZnO have some advantages like thermal and chemical stability and band energy gap 3.37 eV.[4] Most common synthesis of ZnO have a totally oxidation phase without Zn metallic, this occurs either by chemical methods,[5–7] electrochemical[8,9] or sputtering.[10,11] Due to the lack of heterojunctions in a completely oxidized phase, ZnO is usually doped with metals to improve sensing performance[12–14] because of catalytic effect and oxidation resistance. ZnO nanoestructures have a higher surface area for sensing with different morphologies according with the methods and used conditions like needles,[15] belts,[4] wires[16] or rods[17] among others, where very thin structures could have better sensing performance because of greater depletion layer effect.[13]

Furthermore, there are a lot of reports in which Zn metallic thick films are oxidized with thermal treatment, but a lot of them do not take to account that treatments on films upper than 500°C induce fragile layers that break easily due to thermal expansion coefficient,[22] useless on sensors devices. To our knowledge, there is a lack of information about Zn nanostructures as precursor of ZnO because of the melting point of metallic source (419°C). We used a lower temperature range (150-350 °C) with different stages of heating for thermal oxidation than used in other papers that range between 400 and 900°C[18–21] because melt metallic zinc could form other uncontrollable morphologies. Finally, when a lower temperature is used is possible to obtain ZnO with good cristalinity and strong UV emission.[22] The aim of this work was to evaluate the effect of thermal oxidation at low temperature on metallic Zn nanostructured film isothermally and with heating rate.

[a]Corresponding author: pacunaa004@alumno.uaemex.mx

II. EXPERIMENTAL

A. Zn deposition

It was used 250 mg metallic Zn powders from distinct purity (99.995% and 98%, both Aldrich). Zn powders were placed in a molybdenum boat (Mo), once the pressure of the vacuum chamber was pumped to 3 $X10^{-6}$ Torr, the Zn powders were heated with electrical current with a rate of 3 Amp/min until 124 Amp and maintained for 60 min to generate hot zinc vapor. The hot zinc vapor condensed onto substrates at 88 mm of distance on glass 15 mm x 25 mm washed with xylene, acetone and ethanol in ultrasonic bath for 10 minutes.

B. DSC and TGA of Zn and Zn deposition

Tthermo gravimetric analysis (TGA) and differential scanning calorimetry (DSC) were done to analyze physical and chemical properties of Zn films compared with Zn powders (SDT Q 600 TA) on N_2 (99.999 %) and O_2 (99.999 %) with heating rate of 20°C/min with a flow of carrier gas of 100 mL/min.

C. Thermal treatments

Two kinds of heating were used to study the effect of thermal treatment at atmospheric pressure, one named as isothermal (ISO) which means that temperature was almost constant from initial to the final of treatment, and the other with a heating rate (HR) because of the furnace on/off function induce two stages. In the first stage, temperatures reach a maximum for few seconds and in the second stage temperature were maintained. Then 4 treatments were done, two at 150°C (3A150_ISO and 3A150_HR) and at 250°C (3A250_ISO and 3A250_HR) by 3 hours, all followed by slow cooling.

D. Characterization

The metallic and oxidized structures were characterized by field emission scanning electron microscopy (JSM-7401F) with an a acceleration of 5 kV, structural analysis was carried out using transmission electron microscopy (TEM JEM-2200FS) with an acceleration of 200 kV, the crystalline structure of the films was analyzed by an X-ray diffractometer on Bragg-Brentano geometry (XDR, Bruker D8Advances) with CuKα (1.541 A) and Raman spectroscopy was performed with micro-Raman system (LabRam HR 800, Jobin-Yvon-Horiba) using the 632 nm line of a He-Ne laser in a backscattering configuration with a 50x objective (Olympus BX-41).

III. RESULTS AND DISCUSSION

A nanostructured thick film (1-3 μm) was obtained with hexagonal grain and disks morphology (Fig 1(a)). The disks were of different lengths, from 30 nm to 1000 nm, with different thickness. It

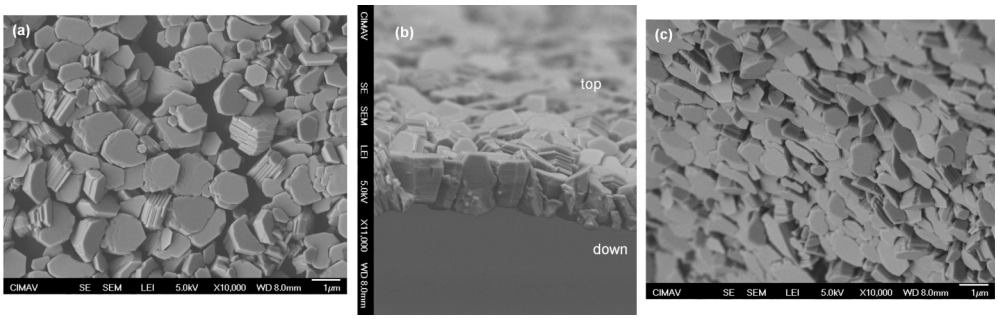

FIG. 1. (a) Top view of Zn metallic film, (b) lateral view and (c) and down or mirror view.

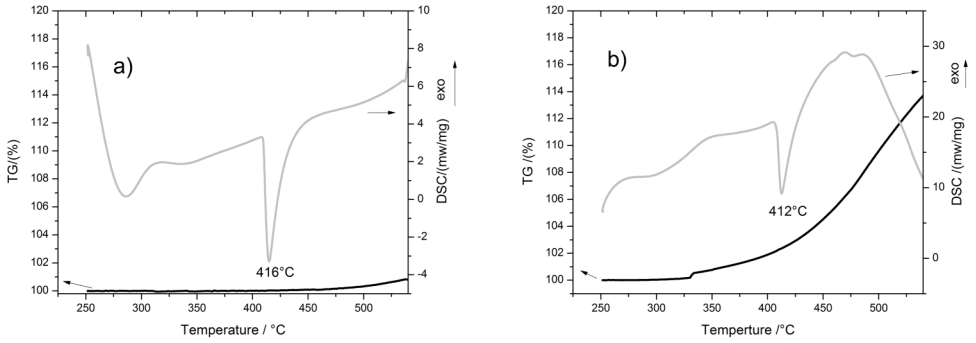

FIG. 2. DSC and TGA under N_2 of a) Zn powder as source material and b) Zn deposited by thermal evaporation.

was observed that disks were grown through very thin disks (10 nm) one after another. The films had poor adhesion to the substrate, as indicated in other papers[26] it was used a strip of adhesive and tape off the film and a lateral view were obtained (Fig 1(b)), at down of the film is observed parallel structures to the substrate (not included) which form a view mirror (Fig 1(c)). On the down view is clearly seen the hexagonal morphology of the disks, but along the growth of the structures, most of them collapse to form grains. Described disks were similar to few reports about metallic Zn nanostructures.[23–25]

The TGA and DSC under N_2 atmosphere was used to found if the melting point of Zn was changed. As can be observed on Fig 2, the endothermic peak on Zn powder was 416°C, and the deposited material reduced the melting point by 4°C. But, indeed another more surprising size effect was observed; apparently oxidation occurs under N_2 atmosphere because of the gain on weight and a wide exothermic peak that indicate reaction not observed with Zn powder.

The zinc was oxidized totally in both samples when an oxidant atmosphere was used (Fig 3). Nevertheless, the start and the end of oxidation temperature were different. Zn powder started the oxidation at approximately after the melting point and finished at 800°C; by the other hand, Zn nanostructures started before the melting point at 314°C where a small exothermic peak was observed, and finished at 597°C. This difference is related with the size of the particles.[18]

On FESEM micrograph 3A150_ISO (Fig. 4(a)) were observed that hexagons are regular with well defined angles and thinner than untreated film. This phenomenon have not been well studied, we believe that at this temperature atoms migrate to form a stable structure, other workers[23] propose that is a nonequilibrium process that can help determine the evolution of the surface morphology and size of the Zn hexagonal nanodisks. Also, have not been studied the change on melting temperature of Zn nanodisks, according to the model proposed by Qi[27] the reduction of melting point on nanostructures is proportional to the atoms on the surface. Taking into account the geometry of nanodisks, the thickness of the disks defines a change on melting point.

When the treatment included a peak on the heating rate of 300°C by few seconds (3A150_HR, Fig 4(b)) was observed a crystal growth of very thin nanoflakes with an average length of 100 nm

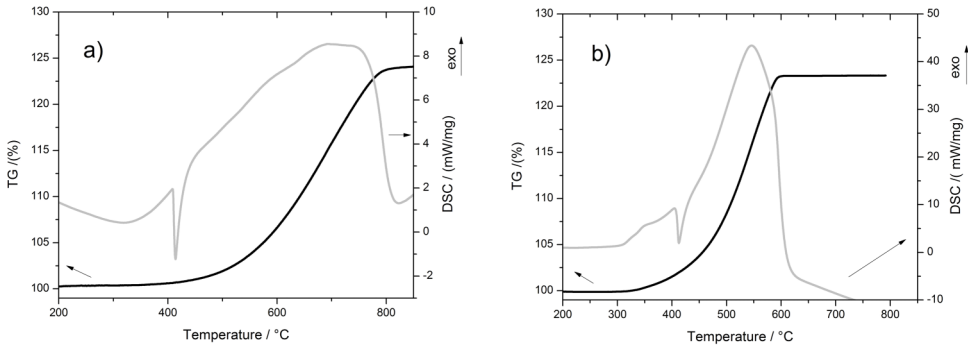

FIG. 3. DSC and TGA under O_2 of a) Zn powder as source material and b) Zn deposited by thermal evaporation.

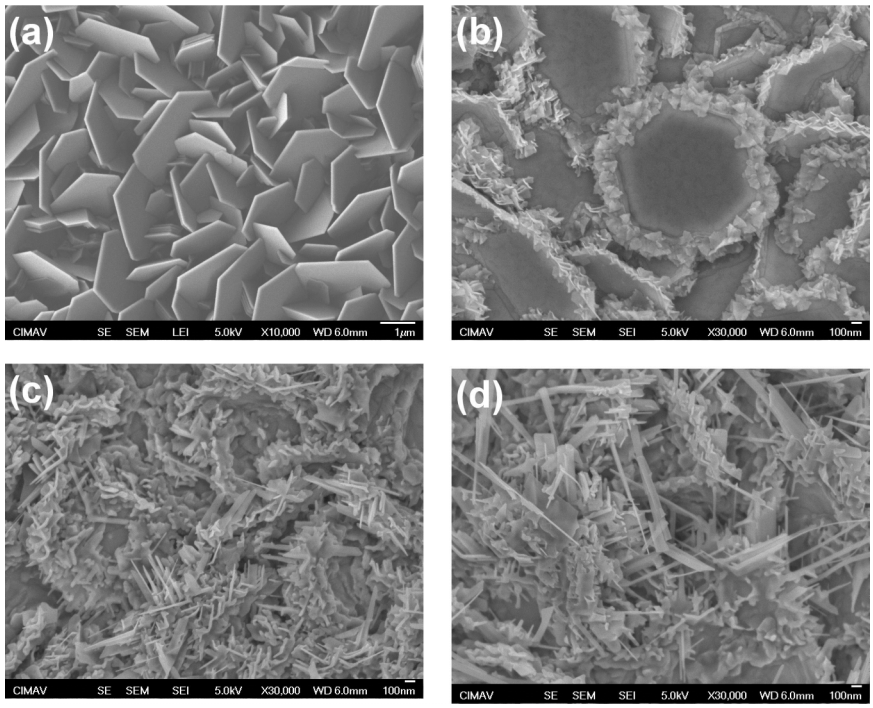

FIG. 4. FESEM images of Zn treated thermally by 3 hours with different conditions: 3A150_ISO (a), 3A150_HR (b), 3A250_ISO(c) and 3A250_HR (d).

with a thickness <20 nm at the edge of the hexagons. The oxidation process started at the edges because it is more stable energetically, this was an epitaxial growth because there were not steric hindrance in other directions,[24] but, neither XRD nor Raman was detected the presence of ZnO perhaps by the detection limit of each technique.

At higher temperature, oxidation was favored in all directions. On FESEM images of 3A250_ISO (Fig 4(c)) nanoneedles were observed with width of 10 to 100 nm and length from 10 to 500 nm, but when a maximum temperature was reached, even by few seconds (3A250_HR, Fig 4(d)) needles were grown a microns on length and some nanobelts were formed.

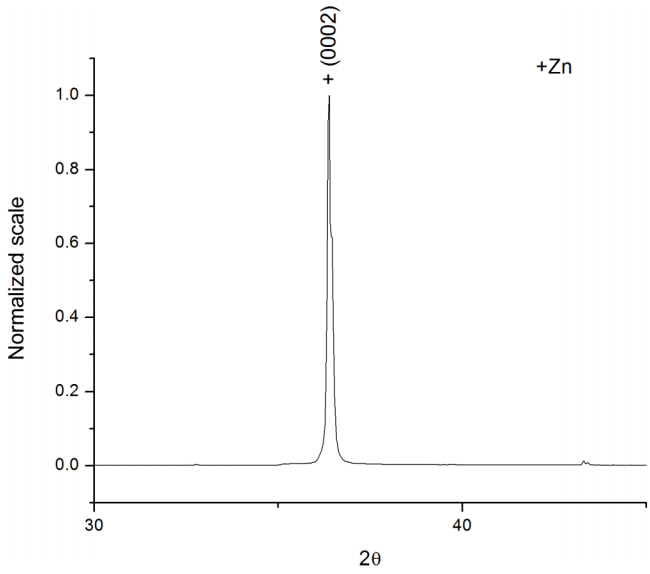

FIG. 5. Diffractogram of deposited Zn nanostructures.

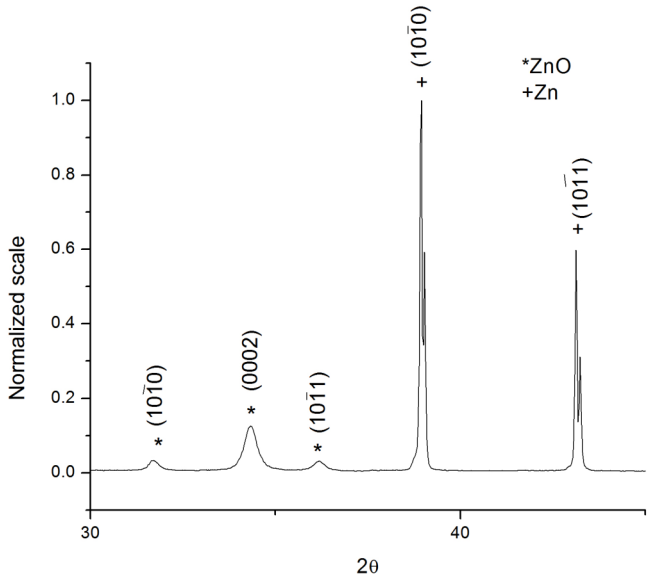

FIG. 6. Diffractogram of Zn thermally treated 3 hours at 250°C.

An XRD analysis of deposited Zn nanodiks indicate (Fig 5) that crystallites were highly oriented to *c*-axis, a strong signal at 2θ=36.52° and a very weak at 2θ=39° corresponding to the planes (0002) and (10$\bar{1}$0) respectively, showing the wurtzite structure with lattice constants of a=b=0.266 nm, c =0.49 nm, α=β=90° and γ=120° (JCPDS card no. 65-3358)

X-ray diffraction detected ZnO in the thermal treatments at 250°C. No differences on crystal structure was detected between ISO an RH treatments, both had 5 peaks, the first three were broad and less intense and the other two were sharp and intense (Fig 6.). The first three signals at 2θ =31.66, 34.34° and 36.15° corresponding to the planes (10$\bar{1}$0), (0002) and (10$\bar{1}$1) respectively, showing the wurtzite structures with lattice constants of a=b=0.326 nm, c=0.522, α=β=90° and γ=120° (JCPDS card no. 36-1451). The sharp and intense peaks at 2θ=39° and 43.21° corresponding to the planes (10$\bar{1}$0) and (10$\bar{1}$1) of metallic Zn respectively (JCPDS card no. 65-3358). Using Sherrer's equation, the broad signals due to ZnO indicate smaller crystallites than the Zn crystallites, calculating the crystallite of ZnO is approximately 20 nm.

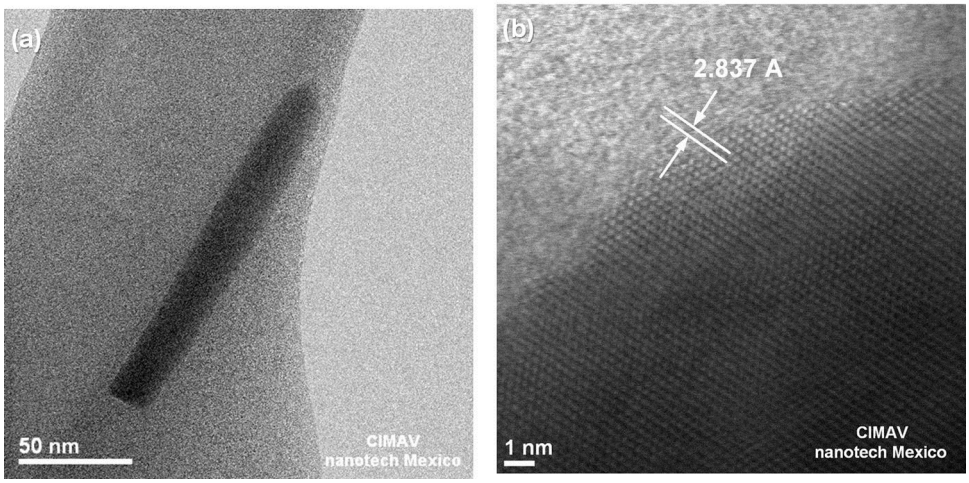

FIG. 7. (a) Nanoneedle extracted from 3A250_ISO and (b) zoom at the edge of the nanoneedle where measure is according to ZnO(10$\bar{1}$0).

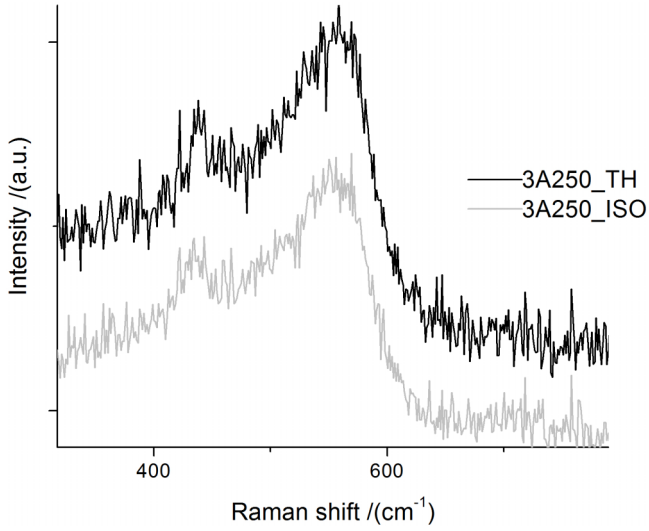

FIG. 8. Scattering Raman spectra of films thermally treated at 250°C.

The XRD of nanoflakes, nanoneedles and nanobelts demonstrated that there were ZnO crystallites that were grown on preferential direction *c*-axis, and there still metallic Zn with different crystalline arrangement compared with Zn-deposition (Fig 5).

TEM was used to examine the crystalline structure of nanoneedles obtained under treatment 3A250_ISO. The high magnification TEM image in Fig 7(a) displays a nanoneedle. The portion of the edge shown in Fig. 7(b) revealed the atomic planes of ZnO ($10\bar{1}0$). This confirms the crystalline structure of ZnO obtained under thermal treatment of Zn nanodisks.

Raman spectra (Fig. 8) confirmed the presence of nanometric crystals of ZnO due to a scatter band between 530 and 580 cm^{-1} which corresponds to vibration mode A1(LO), this mode have been linked with oxygen vacancies, interstitial Zn, or complex defects with oxygen vacancies and interstitial Zn on the ZnO lattice.[10] The vibrational mode E2(High) is intense when the temperature of the thermal treatment is higher than 400°C linked with a higher degree of cristalinity that could be confirmed by XRD with larger crystal size. Therefore, the vibrational band 530-580 cm^{-1} is attributed to the presence of nanometric crystals (<20 nm) on the surface of metallic Zn nuclei.

IV. CONCLUSION

Metallic nanostructured Zn film obtained by thermal evaporation had a lower melting point and lower oxidation temperature than Zn powder and then it was possible to obtain ZnO nanostructures with thermal treatments at temperatures lower than the melting point of Zn. ZnO nanoflakes, nanoneedless and nanobelts were obtained, although similar temperature ranges with different heating stages. The higher temperature was reached, the longer ZnO structures were observed. Finally, Zn/ZnO core/shell structures were obtained when thermal oxidation is performed at 250°C, characterized by smaller crystal size and surface vibrational modes. Optical, electrical and sensing properties are needed to be investigated.

[1] S Wang, P Wang, C Xiao, Z Li, B Xiao, R Zhao, and T. Yang, Mater Lett **131**, 358-60 (2014).
[2] F Pourfayaz, Y Mortazavi, a. Khodadadi, and S. Ajami, Sens Actuators, B **130**, 625-–9 (2008).
[3] Y Kwon, H Kim, S Lee, IJ Chin, TY Seong, and WI. Lee, Sens Actuators, B **173**, 441–6 (2012).
[4] D Zappa, E Comini, and G. Sberveglieri, Nanotechnol **24**, 444008 (2013).
[5] JP Cheng, ZM Liao, D Shi, F Liu, and XB. Zhang, J Alloys Compd **480**, 741–6 (2009).
[6] RC Pawar, J-W Lee, VB Patil, and CS. Lee, Sensors Actuators B Chem **187**, 323–30 (2013).
[7] Y Lv, C Li, L Guo, F Wang, Y Xu, and X. Chu, Sensors Actuators B Chem **141**, 85–8 (2009).
[8] O Lupan, T Pauporté, L Chow, B Viana, F Pellé, and LK. Ono, Appl Surf Sci **256**, 1895–907 (2010).
[9] R. Marotti, Sol Energy Mater Sol Cells **82**, 85–103 (2004).
[10] HQ Bian, SY Ma, FM Li, and HB. Zhu, Superlattices Microstruct **58**, 171–7 (2013).

[11] S Choopun, N Hongsith, P Mangkorntong, and N. Mangkorntong, Phys E Low-Dimensional Syst Nanostructures **39**, 53–6 (2007).
[12] N. Yamazoe, Sensors Actuators B Chem **5**, 7–19 (1991).
[13] N Hongsith, E Wongrat, T Kerdcharoen, and S. Choopun, Sensors Actuators B Chem **144**, 67–72 (2010).
[14] C Wang, L Yin, L Zhang, D Xiang, and R. Gao, Sensors (Basel) **10**, 2088–106 (2010).
[15] I Mihailova, V Gerbreders, E Tamanis, E Sledevskis, R Viter, and P. Sarajevs, J Non Cryst Solids **377**, 212–6 (2013).
[16] O Martínez, V Hortelano, J Jiménez, JL Plaza, S De Dios, J Olvera *et al.*, J Alloys Compd **509**, 5400–7 (2011).
[17] L Zhang and Y. Yin, Sensors Actuators B Chem **183**, 110–6 (2013).
[18] Y Gui, CX Ã, Q Zhang, M Hu, J Yu, and Z. Weng, J Cryst Growth **289**, 663–9 (2006).
[19] Q Xu, Q Cheng, Z Zhang, R Hong, X Chen, Z Wu *et al.*, J Alloys Compd **590**, 260–5 (2014).
[20] C Lin and L. Chao, ZnO. IEEE 10–1 (2010).
[21] MR Khanlary, V Vahedi, and A. Reyhani, Molecules **17**, 5021–9 (2012).
[22] J Zhao, L Hu, Z Wang, Y Zhao, X Liang, and M. Wang, Appl Surf Sci **229**, 311–5 (2004).
[23] RS Devan, J-H Lin, Y-J Huang, C-C Yang, SY Wu, Y Liou *et al.*, Nanoscale **3**, 4339–45 (2011).
[24] S Cho and K-H. Lee, Cryst Growth Des **10**, 1289–95 (2010).
[25] RK Gupta, N Shridhar, and M. Katiyar, Mater Sci Semicond Process **5**, 11–5 (2002).
[26] NJ Simrick, JA Kilner, and A. Atkinson, Thin Solid Films **520**, 2855–67 (2012).
[27] R Kumar and M. Kumar, Indian J Pure Appl Phys **50**, 329–34 (2012).